PCCP

Accepted Manuscript

ROYAL SOCIETY OF CHEMISTRY

www.rsc.org/pccp

Table of contents entry

This study examines structures of all plausible terminations of $CuCl_2$ surfaces and assess their thermodynamic stability under practical operational conditions, relevant to the role of $CuCl_2$ as the most crucial chlorination catalysts in combustion systems.

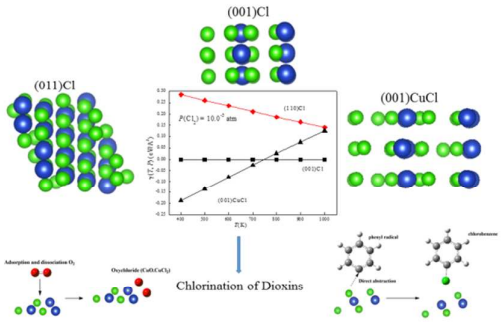

Structures and Thermodynamic Stability of Copper(II) Chloride Surfaces

Mohammednoor Altarawneh*†, Bogdan Z. Dlugogorski, Zhong-Tao Jiang

School of Engineering and Information Technology

Murdoch University, Perth, Australia

*Corresponding Author:

Phone: (+61) 8 9360-7507

E-mail: M.Altarawneh@Murdoch.edu.au

† On leave from Chemical Engineering Department, Al-Hussein Bin Talal University, Ma'an, Jordan

Abstract

Using density functional theory calculations of periodic slabs, within the generalised gradient approximation, this study provides optimised structures for all plausible terminations of copper(II) chloride surfaces along the three low-index orientations. The ab initio atomistic thermodynamic approach serves to construct a thermodynamic stability diagram for $CuCl_2$ configurations as a function of chemical potential of chlorine ($\Delta\mu_{Cl}(T,p)$). We observe a shift in thermodynamic stability ordering at around $\Delta\mu_{Cl}(T,p)$ = -1.0 eV between a copper-chlorine terminated (001) surface (i.e., (001)CuCl), and a (001) chlorine-covered surface (i.e., (001)Cl). This conclusion accords with experimental observations that report CuCl-bulk like structures, acting as prerequisite for the formation of $CuCl_2$-bulk like arrangements in the course of copper chlorination. Profound stabilities and optimised structures of (001)CuCl and (001)Cl configurations are discussed within the context of the functionality of $CuCl_2$ as the chief chlorination and condensation catalyst of aromatic pollutants under conditions relevant to their formation in thermal systems, i.e. 400 – 1000 K, total operating pressure of 1.0 atm and $p_{Cl2} = 10^{-6} – 10^{-4}$ atm (1.0 – 100.0 ppm).

1. Introduction

The interaction of chlorine with copper has been in the centre of mounting experimental and theoretical research, as a consequence of the importance of this interaction for formation of aromatic pollutants. In situ surface analytical techniques [1,2] surveyed adsorption of chlorine on clean copper surfaces and subsequent diffusion of chlorine into the copper bulk. Results from scanning tunnelling microscopy (STM) [3] confirmed the formation of a *c*(2×2) chemisorbed chlorine layer immediately upon the exposure of a Cu(100) surface to a gaseous Cl_2. Along the same line of enquiry, several studies [4-6] have pointed out the formation of a thin copper(I) chloride (CuCl) film from adsorption of chlorine on a Cu(100) surface. De Micco et al. [4] performed a thermogravimetric (TG) study on copper chlorination under different temperature conditions. Their Ellingham diagrams projected the formation of CuCl as the initial copper chlorination product. Copper(II) chloride ($CuCl_2$) was regarded as the predominant final species in the Cu(100)/Cl system [7]. Mechanistically, formation of CuCl is often considered as prerequisite to the appearance of $CuCl_2$ [4,7,8]. Evolution of $CuCl_2$ via direct substitutional chlorine adsorption was found to incur a considerable thermodynamic penalty if compared with the more preferred surface adsorption [9]. Li et al. [10] observed a nominal coverage of 4/5 ML corresponding to (1×5)-Cl/Cu(110) structures. LEED measurements by Walter et al. [11] demonstrated that adsorption of chlorine on a Cu(111) commences with the sublimation of CuCl and $CuCl_2$ species.

Theoretically, Suleiman et al. [12] proposed a shape of copper nano-structure surrounded by a gaseous chlorine environment, by performing the Wulff construction. But under practical values of the chemical potential of chlorine, bulk CuCl constitutes the thermodynamically most stable copper-chlorine configuration. Thus, consensus of opinions from experimental

measurements and theoretical predictions illustrates that, copper chlorides resemble limiting cases for adsorption of chlorine on copper surfaces.

$CuCl_2$, in particular, has been demonstrated to be a potent chlorinating catalyst in the course of the formation of chlorinated aromatics, most notably a group of the notorious dioxin-like species [13]. The majority of copper content in fly ash exists as $CuCl_2$ [14]. In heterogeneous formation of dioxins, $CuCl_2$ plays a prominent role, not only as a chlorine source, but also in mediating the occurrence of prominent chemical reactions [15]. $CuCl_2$ is a primary intermediate in the so-called Deacon reaction [16-18] which converts the inert HCl gases into the active Cl_2 chlorination species. Despite the importance of $CuCl_2$ as a final product from the interaction of gaseous chlorine with copper surfaces and its role in the formation of chlorinated organic pollutants, the literature lacks an atomic-based description of $CuCl_2$ surfaces. To this end, the aim of this contribution is to examine structures of all plausible terminations of $CuCl_2$ surfaces and to assess their thermodynamic stability under practical operational conditions, relevant to the role of $CuCl_2$ as the most crucial chlorination catalysts in combustion systems.

2. Computational details

2.1. Structural optimisation

All structural and energetic calculations comprise the spin-polarised PAW-GGA functional [19] as implemented in the VASP code [20]. We simulate various $CuCl_2$ surfaces using 2 by 2 surface supercells consisting of 10 to 23 symmetric-slab layers (containing 26 to 58 atoms).

The presence of two outermost layers in symmetric slabs (i.e., symmetrical staking sequence) largely minimises effects of dipole moment that might accumulate along the *z*-direction [21]. Chlorine-terminated surfaces may exhibit a weak polar characteristic, however, utilisation of symmetric slabs eliminates any surface deformation derived by dipole moment perpendicular to the surface. All atomic layers are allowed to relax while keeping the innermost 1-3 layers fixed at their bulk positions. Vertical vacuum regions of 12.0 Å to 20.0 Å separate the adjacent slabs along the two sides of symmetric slabs. Energy cut-off is set at 400 eV in all simulations and the Monkhorst-Pack (MP) [22] grids serve to perform the Brillouin zone (BZ) integration. MP schemes generate 9-10 **k**-points in the irreducible part of the BZ for all surfaces. An energy cut-off of 500 eV and 16 **k**-points change the total energy of the (001)Cl surface (see Section 3.2) marginally by 26.3 meV, i.e. 0.30 %. The precision of total energies and forces on each ion converge to 10^{-4} eV and 0.02 eV $Å^{-1}$, respectively.

2.2. Thermodynamic stability

We construct a thermodynamic stability phase diagram encompassing all $CuCl_2$ configurations based on the approach of *ab initio* atomistic thermodynamics. Literature provides detailed descriptions pertinent to this approach [23-26]. Herein, we briefly refer to the governing equations. In this formalism, surface free energies, at a given temperature and pressure, $\gamma(T,P)$, linearly relate to the chemical potential of chlorine, $\mu_{\mathrm{Cl}}(T,P)$, via:

$$\gamma(T,P)=\frac{1}{2A}\left[G^{Surf}(T,P)-N_{\mathrm{Cu}}g^{\mathrm{Bulk}}_{\mathrm{CuCl_2}}(T,P)-(N_{\mathrm{Cl}}-2N_{\mathrm{Cu}})\mu_{\mathrm{Cl}}(T,P)\right] \quad (1)$$

where A, $G^{Surf}(0\,\mathrm{K},1\,\mathrm{atm})$, $g^{\mathrm{Bulk}}_{CuCl_2}$, N_{Cu} and N_{Cl} signify surface area, calculated Gibbs energy of a $CuCl_2$ surface, Gibbs energy of bulk $CuCl_2$ per unit formula and numbers of copper and chlorine atoms in the $CuCl_2$ surface, in that order. Finally, $\mu_{Cl}(T,P)$ is expressed as:

$$\mu_{Cl}(T,p) = \Delta\mu_{Cl}(T,p) + 1/2E_{Cl_2} \qquad (2)$$

where $\Delta\mu_{Cl}(T,p)$ and E_{Cl_2} refer to the change in chlorine chemical potential and the internal energy of an isolated chlorine molecule, respectively. Values of the chlorine chemical potential are estimated from standard thermodynamic tables [27].

The two Gibbs terms in Equation (1) comprise enthalpic (H) and entropic (S) terms:

$$G = H - TS \qquad (3)$$

The total H value of a system comprises contribution from total energy of the system at 0 K and 1 atm, (E^{tot}), vibrational energy (F^{vib}) and a pressure-volume term (PV). Thus, Equation 3 can be written as:

$$G = E^{tot} + F^{vib} + PV - TS \qquad (4)$$

Electronic structure calculations provide the value of the E^{tot} term, typically at 0 K and 0 atm. By applying a simple dimensional analysis on the PV term, it is revealed that, its contribution to the total G value will be less than 0.1 meV/Å^2. This value is a rather negligible if compared with the magnitude of E^{tot}. Thus, the PV term in Equation (4) could be safely ignored. In well-ordered configurations, such as solid state systems, the contribution of the TS term is minimal and can be neglected as well. Consensus of theoretical predictions from the literature [25,28] points out that the contribution of the F^{vib} falls within ± 5.0 meV/Å^2, a

value still negligible with respect to the E^{tot} term. It follows that, Equation (4) for a solid surface can be written as:

$$G = E^{tot} \quad (5)$$

Finally, substitution of Equation (5) in Equation (1) results in the following governing equation of the *ab initio* atomistic thermodynamics:

$$\gamma(T,P) = \frac{1}{2A}\left[E^{tot}(0\text{ K},1\text{ atm}) - N_{Cu}E^{Bulk}_{CuCl_2}(0\text{ K},1\text{ atm}) - (N_{Cl} - 2N_{Cu})\mu_{Cl}(T,P)\right] \quad (6)$$

3. Results and discussion

3.1. Bulk $CuCl_2$

A unit cell of bulk $CuCl_2$ exists as a base-centred monoclinic Bravais lattice, in which each Cu atom lies at the centre of an axially distorted octahedral arrangement composed of six chlorine atoms; see Figure 1. Optimisation of bulk $CuCl_2$ unit cell is carried out by deploying a 6×6×6 MP automatic generation of **k**-points and an energy cut-off at 600 eV. Figure 1 depicts an optimised structure of a $CuCl_2$ unit cell. Our estimated lattice constants (7.201 Å, 3.371 Å and 7.356 Å) are in a relatively good agreement with corresponding experimental measurements (6.900 Å, 3.300 Å and 6.820 Å) [29] and other theoretical predictions (7.520 Å, 3.3350 Å and 7.290 Å) [30]. The noticeable difference between calculated and experimental *c* lattice constant attributes to the fundamental shortcoming of DFT functionals in describing states that encompasses long-range interactions [31]. Figure 1 lists the nearest

bulk Cu/Cl distances in addition to Cl-Cl (4.207 Å) and Cu-Cu (7.356 Å) intra-layer spacings.

3.2. *Geometries of $CuCl_2$ surfaces*

We consider all plausible $CuCl_2$ surface configurations. Surface terminations of $CuCl_2$ afford seven non-equivalent low-index orientations, namely, (100), (010), (001), (110),-(101), (011) and (111). The (001) and (110) surfaces exhibit two distinct terminations depending on whether they end with only Cl atoms or a combination of Cl and Cu atoms in their outermost layers. In the subsequent discussion, surfaces carry labels with respect to their orientations and atomic-type termination. For example, (011)CuCl and (001)Cl surfaces denote constructions that are truncated with both Cl/Cu atoms and only Cl atoms in their outermost layers, respectively. Figures 2 and 3 portray optimised structures of $CuCl_2$ with prominent atomic distances and relaxations pertinent to intra-layer Cu-Cu/Cl-Cu spacings presented in Table 1. The comparison between bulk data (Figure 1) and surface geometries (Table 1) reveals that, all $CuCl_2$ surfaces exhibit, to large extent, analogous geometrical features of bulk $CuCl_2$; i.e., surface reconstructions and relaxations are minimal in all surfaces. Generally, all Cu/Cl distances are within 8.5 % of their corresponding bulk distances, see Table 1. Optimised structures of the (001)CuCl and (110)CuCl configurations indicate that Cu-terminated surfaces are not stable. Both surfaces initially contain only Cu atoms at their topmost layers, whereas their optimised minimum energy structures display a downward displacement of Cu atoms forming Cu/Cl-terminated surfaces. The (010)CuCl surface, in particular, exhibits adjacent vertically separated rows of chlorine and copper. Copper and chlorine atoms in the (001)CuCl and (100)CuCl surface lie in a horizontal plane

characterising a CuCl surface-like configuration, while the (101)CuCl and (110)CuCl constitute Cu-Cl inclined sheets. The tendency of $CuCl_2$ surface to exist either as chlorine or chlorine-copper terminated-configurations suggests a weak polar-induced behaviour of these surfaces. One deduces from numbers in Table 1 that, intra-layer Cu-Cu and Cl-Cl spacings in all surfaces deviate marginally from their corresponding bulk values Supplementary Information (SI) provides Cartesian coordinates of all $CuCl_2$ surfaces.

3.3 Stability phase diagram

In practical scenarios, $\Delta\mu_{Cl}(T,P)$ lay between two limits, namely chlorine-lean and chlorine-rich boundaries [25,26]. In physical terminology, a chlorine-lean limit denotes the commencement of the formation of a $CuCl_2$ bulk upon the presence of copper bulk in a phase reservoir of chlorine gas, whereas a chlorine-rich limit signifies condensation of gaseous Cl_2 molecule. As a well- defined estimate, the later term is considered to be half of the total energy of a chlorine molecule. On the scale of $\Delta\mu_{Cl}(T,P)$, chlorine-lean and chlorine-rich conditions are assigned a value of $\Delta_f H^o_{298}$ for $CuCl_2$ (i.e. -2.28 eV) [32] and a zero. Table 2 lists values of $\gamma(T,P)$ at the considered boundaries. Between these two physically-meaningful limits, equilibrium calculations yield results of practical significance. Figure 4 explores trends in $\gamma(T,P)$ with the gradual increase in $\Delta\mu_{Cl}(T,P)$. Under very dilute chlorine content and up to $\Delta\mu_{Cl}(T,P)$ of -1.0 eV, the stability of the (001)CuCl is easily recognised. Over the narrow $\Delta\mu_{Cl}(T,P)$ range of -1.0 eV to 0.5 eV, the fully chlorine-covered (001)Cl surface becomes thermodynamically the most stable configuration.

The transition to the stable configuration from the (001)CuCl surface to the (001)Cl is intuitively very appealing. It infers two focal points. Firstly, reactive surface Cu atoms in the (001)CuCl are able to adsorb more chlorine atoms at experimentally accessible conditions; thus, shuttling between Cu(I) and Cu(II) oxidation states. Secondly, the transitions from CuCl-bulk like structure of (001)CuCl to the $CuCl_2$-bulk like structure of (001)Cl is consistent with the experimental findings [4,7] that CuCl bulk constitutes a prerequisite, or an intermediate, for the formation of $CuCl_2$. In a recent theoretical study, Suleiman et al. [9] indicated that, a (001)Cl-like structure could potentially be formed via a 2ML substitutional chlorine adsorption. While the latter configuration appeared to be less stable than the surface adsorption, the authors concluded that its formation might still be kinetically accessible under very rich chlorine conditions.

Beyond $\Delta\mu_{Cl}(T,P)$ of 0.5 eV (i.e. ~ onset of unrealistic values), the stability ordering is predicted to be dominated by the (110)Cl termination. Surprisingly, the three most stable surfaces are chlorine deficient (i.e. their R (Cl/Cu) ≤ 1.0). This indicates that the profound stability of the (001)Cl surface over the viable $\Delta\mu_{Cl}(T,p)$ range (-1.0 – 0.0 eV) stems from its chlorine-covered termination rather than its total chlorine content. The high stability of the chlorine-covered (001)Cl and (110)Cl terminations at experimentally accessible conditions of $\Delta\mu_{Cl}(T,P)$ agrees well with findings of ab initio atomistic studies that have consistently concluded that the oxygen-covered terminations afford the most stable surfaces of CuO [33] and PdO [34].

3.4 Implications for catalytic chlorination of aromatic compounds

As demonstrated earlier, $CuCl_2$ species are the chief chlorination catalysts of aromatic compounds. $CuCl_2$ acts as a chlorinating agent in the two heterogeneous pathways of the formation of dioxins: de novo synthesis (i.e. oxidation of the carbon matrix) and catalytically-mediated coupling of gas phase precursors. Thus, it is insightful to magnify the phase diagram presented in Figure 4 to demonstrate conditions relevant to the chlorination mechanism of dioxins. Formation and subsequent chlorination of dioxins compounds occur in a temperature window of 400 K-1000 K (typically, from 500 K to 750 K) [15]. To the best of our knowledge, no literature data exist that provide direct measurements for the concentrations of Cl_2 in thermal systems relevant to formation of dioxins, such as municipal waste incinerations (MWI). Thermodynamic equilibrium calculations from literature [27] as well as our own computations reveal that the total chlorine speciation occurs mainly as Cl_2. However, kinetics calculations predict that, the chlorine content predominantly transforms into HCl (~ 95.0%) and that Cl_2 contributes by only ~ 1.0% to the overall chlorine speciation [28].

In their experimental study on the formation of dioxins from MWI, Wikström et al. [29] utilised a Cl_2 concentration in the range of 50 ppm – 400 ppm to account for the load of molecular chlorine. On the other hand, concentration of HCl during combustion of various types of coal varies between 25.0 ppm and 110.0 ppm [28]. With the presence of potent chlorine sources in a typical municipal waste incinerator, such as NaCl and polyvinyl chloride (PVC), one could assume the concentration of HCl in MWI to be significantly higher than that in coal combustion. Accordingly, it is sensible to assume that Cl_2 concentrations in MWI could reach as high as 100 ppm throughout the above-mentioned

temperature window. Nevertheless, to account for the plausible significant variations in the actual Cl_2 content in a conventional MWI operation, we plot a *T*-dependent stability phase diagram for the three most stable $CuCl_2$ surfaces using two P_{Cl2} values, 1 ppm (10^{-6} atm) and 100 ppm (10^{-4} atm). Figure 5a and Figure 5b depict $\gamma(T,P)$ for the three most stable surfaces as a function of temperature at 1.0 ppm and 100.0 ppm, correspondingly.

Interestingly, narrow $\Delta\mu_{Cl}(T,P)$ ranges in Figure 5a (-1.69 eV - -0.62 eV) and Figure 4b (-1.49 eV - 0.53 eV) coincide with the transition in thermodynamic stability reported in Figure 3. Clearly, the (001)Cl surface remains more stable than the (110)Cl structure up to ~ 800 K and P_{Cl2} = 1.0 ppm. The transition temperature reduces to ~ 740 K upon an increase of chlorine concentration to 100.0 ppm. However, note that, the very narrow range of $\gamma(T,P)$ for the three surfaces in Figure 5 is most likely to be within the accuracy margin of our calculations and that the nanoparticles with their shapes defined by the three surfaces co-exist under these *T*-*P* conditions.

The effect of exact surface functionality of $CuCl_2$ on the chlorination mechanisms of organic pollutants remains not fully demonstrated. Optimised structures of nanoparticles constrained by the three most stable surfaces, i.e., (001)Cl, (110)Cl and (001)CuCl, could provide insightful elucidation into previously suggested reaction pathways [15,17]. For instance, atoms in the (001)Cl structure are easily accessible to incoming gas phase molecules and radicals:

Scheme 1

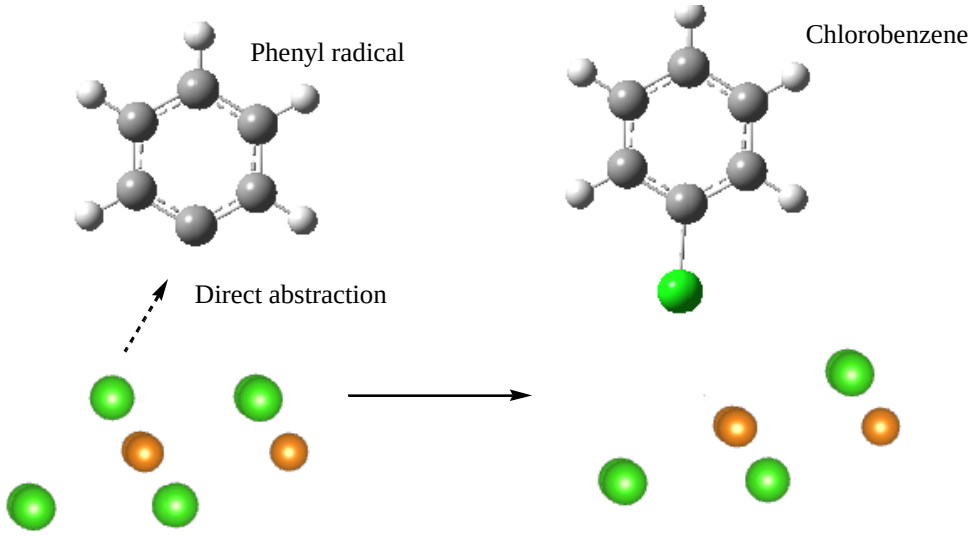

On the other hand, adsorption of molecular oxygen on $CuCl_2$ surface, as the first step in oxychlorination cycle, would have been hindered if the $CuCl_2$ surface had not been fully covered with chlorine. The presence of surface Cu atoms in the (001)CuCl could facilitate the formation of an oxychloride; i.e., a key intermediate in the oxychlorination cycle:

Scheme 2

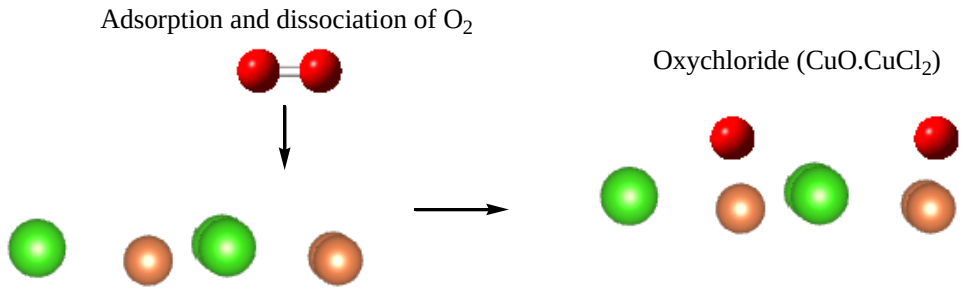

4. Conclusions

We have shown that, optimised structures of all $CuCl_2$ surface terminations resemble the corresponding geometries of bulk $CuCl_2$. Initial arrangements terminated with only Cu atoms in their topmost layers experience a downward replacement of Cu atoms indicating that Cu-truncated surfaces of $CuCl_2$ are not stable. We found that, three structures dominate the *T-p* stability diagram of $CuCl_2$; namely, (001)CuCl at $\Delta\mu_{Cl}(T,P) \leq$ -1.0 eV, (001)Cl for $\Delta\mu_{Cl}(T,P)$ between -1.0 eV and 0.50 eV and (110)Cl for $\Delta\mu_{Cl}(T,P) \geq 0.5$ eV. Under the relevant *T-p* conditions, practical systems are expected to contain nano-particles of $CuCl_2$ terminated with the three types of surfaces. Thus, (001)CuCl, (001)Cl and (110)Cl surfaces play a key role as the main chlorination and condensation catalysts during the formation of aromatic pollutants.

Supplementary Information Available

Cartesian coordinates for all $CuCl_2$ structures.

Acknowledgement

This study has been supported by a grant of computing time from the National Computational Infrastructure (NCI), Australia as well as funds from the Australian Research Council (ARC).

References

[1] W. Sesselmann, T.J. Chuang, Sur. Sci. 176 (1986) 67.
[2] W. Sesselmann, T.J. Chuang, Sur. Sci. 176 (1986) 32.
[3] M. Galeotti, B. Cortigiani, M. Torrini, U. Bardi, B. Andryushechkin, A. Klimov, K. Eltsov, Surf. Sci. 349 (1996) L164.
[4] G. De Micco, A.E. Bohé, D.M. Pasquevich, J. Alloys. Compd. 437 (2007) 351.
[5] C.Y. Nakakura, V.M. Phanse, E.I. Altman, Surf. Sci. 370 (1997) L149.
[6] C.Y. Nakakura, G. Zheng, E.I. Altman, Surf. Sci. 401 (1998) 173.
[7] H.C.N. Tolentino, M. De Santis, Y. Gauthier, V. Langlais, Surf. Sci. 601 (2007) 2962.
[8] J.W. Krewer, R. Feder, A. Baalmann, A. Goldmann, J. Phys. C-Solid State Phys. 20 (1987) 2041.
[9] I.A. Suleiman, M.W. Radny, M.J. Gladys, P.V. Smith, J.C. Mackie, E.M. Kennedy, B.Z. Dlugogorski, Phys. Chem. Chem. Phys. 13 (2011) 10306.
[10] W.H. Li, Y. Wang, J.H. Ye, S.F.Y. Li, J. Phys. Chem. B 105 (2001) 1829.
[11] W.K. Walter, R.G. Jones, J. Phys: Condens. Matter 1 (1989) SB201.
[12] I.A. Suleiman, M.W. Radny, M.J. Gladys, P.V. Smith, J.C. Mackie, E.M. Kennedy, B.Z. Dlugogorski, J. Phys. Chem. C 115 (2011) 13412.
[13] J.-Y. Ryu, J.A. Mulholland, M. Takeuchi, D.-H. Kim, T. Hatanaka, Chemosphere 61 (2005) 1312.
[14] M. Takaoka, A. Shiono, K. Nishimura, T. Yamamoto, T. Uruga, N. Takeda, T. Tanaka, K. Oshita, T. Matsumoto, H. Harada, Environ. Sci. Technol. 39 (2005) 5878.
[15] M. Altarawneh, B.Z. Dlugogorski, E.M. Kennedy, J.C. Mackie, Prog. Energy. Combust. Sci. 35 (2009) 245.
[16] M. Mortensen, R.G. Minet, T.T. Tsotsis, S.W. Benson, Chem. Engi. Sci. 54 (1999) 2131.
[17] M.W.M. Hisham, S.W. Benson, J. Phys. Chem. 99 (1995) 6194.
[18] U. Nieken, O. Watzenberger, Chem. Engi. Sci. 54 (1999) 2619.
[19] J.P. Perdew, K. Burke, Y. Wang, Phys. Rev. B. 54 (1996) 16533.
[20] G. Kresse, J. Furthmüller, Phys. Rev. B. 54 (1996) 11169.
[21] P.W. Tasker, J. Phys. C: Solid State Phys. 12 (1979) 4977.
[22] H.J. Monkhorst, J.D. Pack, Phys. Rev. B. 13 (1976) 5188.
[23] J. Rogal, K. Reuter, M. Scheffler, Phys. Rev. Lett. 98 (2007) 046101.
[24] C. Stampfl, Catal. Today 105 (2005) 17.
[25] K. Reuter, M. Scheffler, Phys. Rev. B. 65 (2001) 035406.
[26] W.-X. Li, C. Stampfl, M. Scheffler, Phys. Rev. B. 68 (2003) 165412.
[27] M.W. Chase, NIST-JANAF thermochemical tables, American Chemical Society ; American Institute of Physics for the National Institute of Standards and Technology, [Washington, D.C.]; Woodbury, N.Y., 1998.
[28] K. Reuter, M. Scheffler, Phys. Rev. Lett. 90 (2003) 046103.
[29] P.C. Burns, F.C. Hawthorne, Am. Mineral 78 (1993) 187.
[30] S. Peljhan, A. Kokalj, J. Phys. Chem. C. 113 (2009) 14363.
[31] O.A. von Lilienfeld, I. Tavernelli, U. Rothlisberger, D. Sebastiani, Phys. Rev. Lett. 93 (2004) 153004.
[32] RC handbook of chemistry and physics: a ready-reference book of chemical and physical data, CRC, Boca Raton, London, 2008.
[33] A. Soon, M. Todorova, B. Delley, C. Stampfl, Phys. Rev. B. 75 (2007) 125420.
[34] J. Rogal, K. Reuter, M. Scheffler, Phys. Rev. B. 69 (2004) 075421.

366 **Table 1**: Selected distances (in Å) and surface relaxations (with respect to bulk Cu-Cu and

367 Cl-Cu intra-layer spacings).

	Cu-Cl	Cu-Cu	Cl-Cl	Cu-Cu (%)	Cl-Cl (%)
(100)Cl	2.308, 3.315	3.371	3.371	0.67	1.69
(110)Cl	2.295	3.371, 3.975	3.151		
(001)CuCl	2.234, 3.193	3.371	3.371		
(110)CuCl	2.351	3.372	3.371		
(010)CuCl	2.323	3.746	3.206	0.00	-0.71
(100)CuCl	2.295, 3.418	3.371	3.371	0.95	5.85
(101)CuCl	2.294, 3.151	3.371	3.371	0.95	5.85
(111)CuCl	2.291, 3.143	3.984	3.14	8.22	-0.36
(011)CuCl	2.321	3.371	3.122		

368

369

370

371 **Table 2**: Surface adsorption energies and chlorine/copper ratios.

		γ(eV/A^2)	
Surface	*R* (Cl/Cu)	Chlorine-lean limit	Chlorine-rich limit
(100)Cl	2.0	0.00	0.00
(110)Cl	2.2	-0.21	0.14
(001)CuCl	1.6	0.88	0.13
(110)CuCl	1.8	0.58	0.23
(010)CuCl	2.0	0.07	0.07
(100)CuCl	1.9	0.20	0.02
(101)CuCl	2.2	-0.08	0.14
(111)CuCl	2.0	0.09	0.09
(011)CuCl	2.1	0.00	0.08

372

373

374

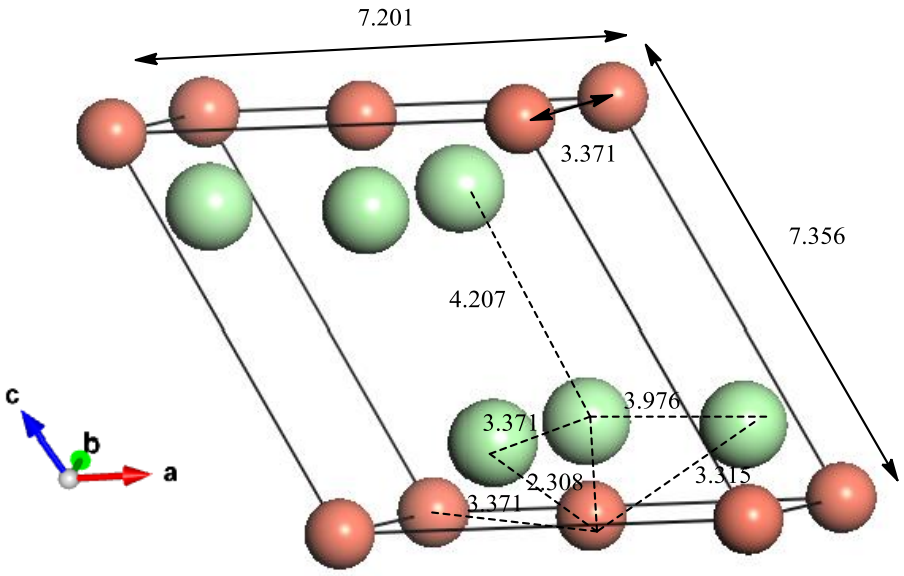

375

376 **Figure 1:** Optimised $CuCl_2$ unit cell. Distances are in Å. Chlorine atoms are denoted by

377 larger green-coloured spheres.

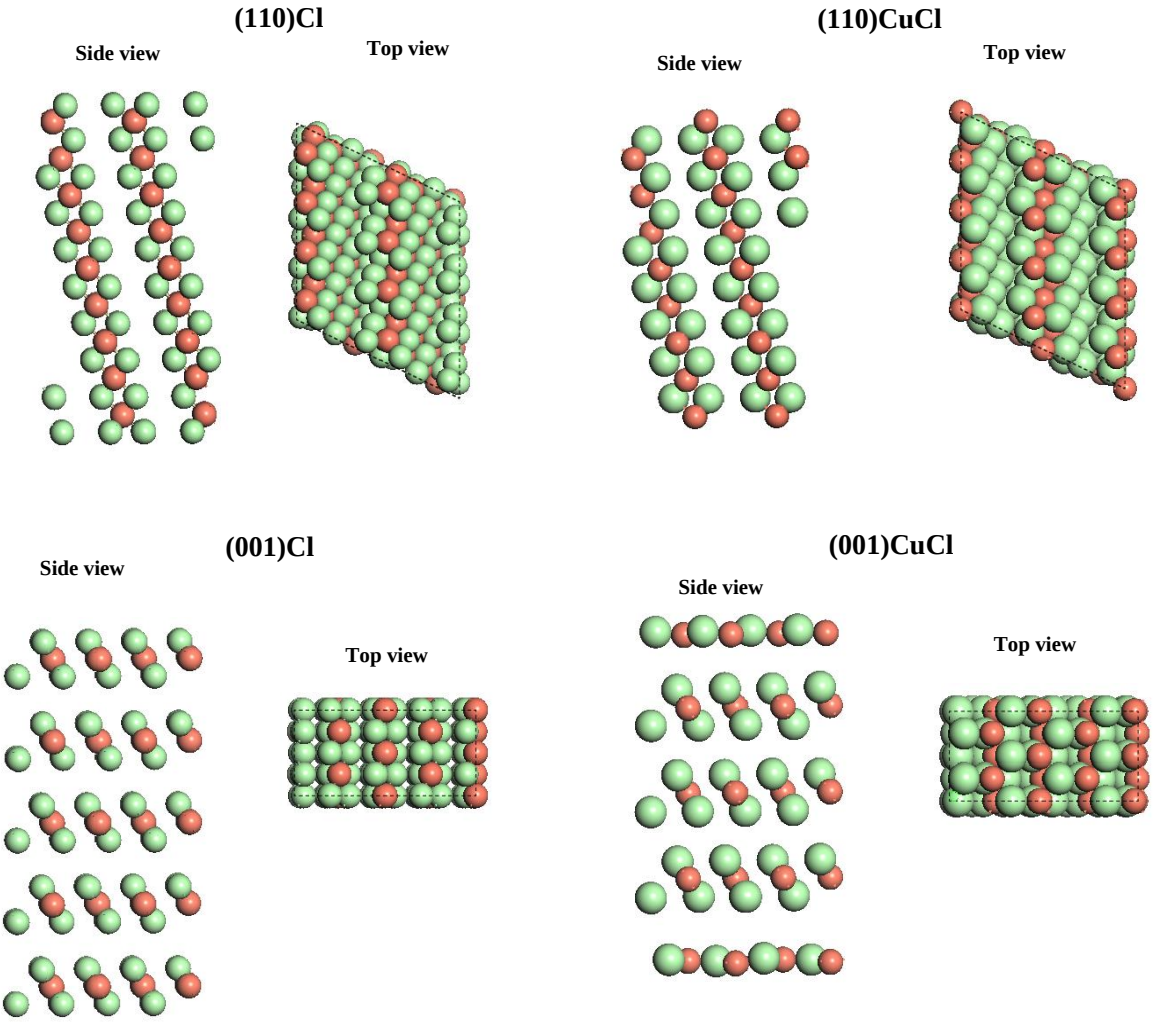

Figure 2: Optimised geometries of (110)Cl, (110)CuCl, (001)Cl and (001)CuCl $CuCl_2$ surfaces. Chlorine atoms are denoted by larger green-coloured spheres.

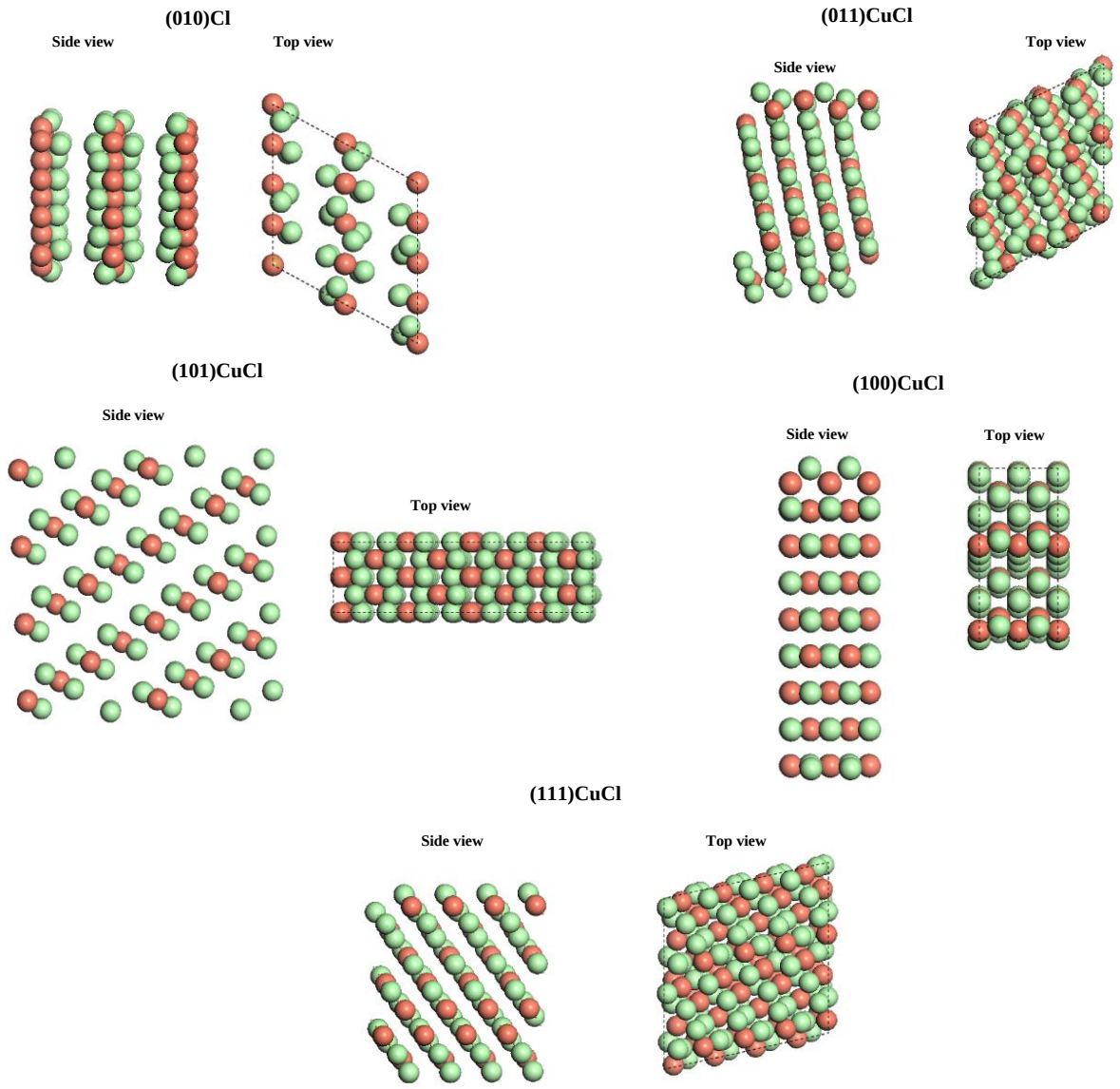

Figure 3: Optimised geometries of (010)CuCl, (011)CuCl, (101)CuCl, (100)CuCl and (111)CuCl surfaces. Chlorine atoms are denoted by larger green-coloured spheres.

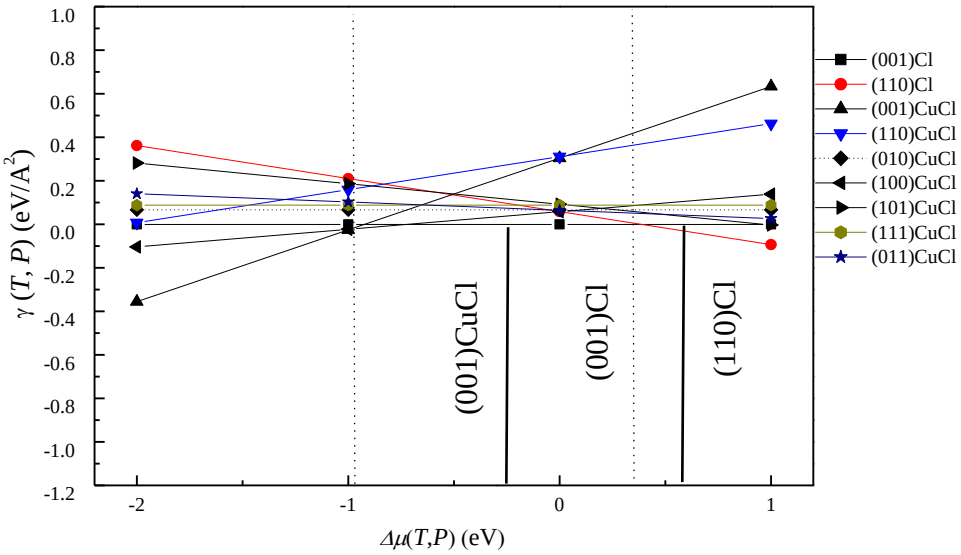

395

396 **Figure 4**. Surface free energies of $CuCl_2$ surfaces as a function of the chemical potential of

397 chlorine.

398

399

400

401

402

403

404

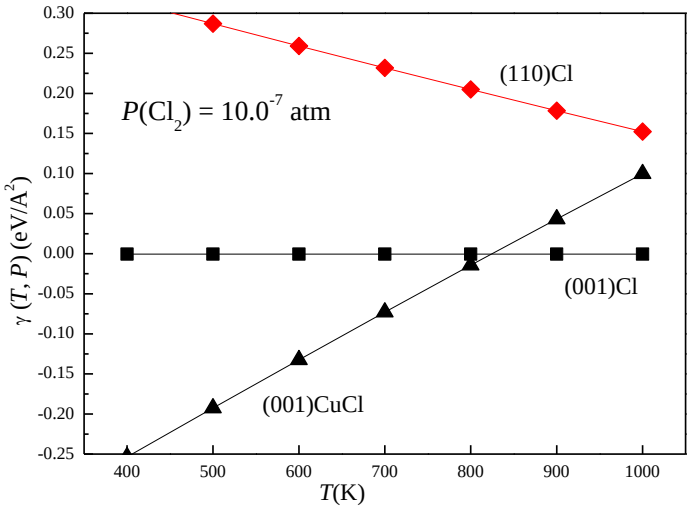

405

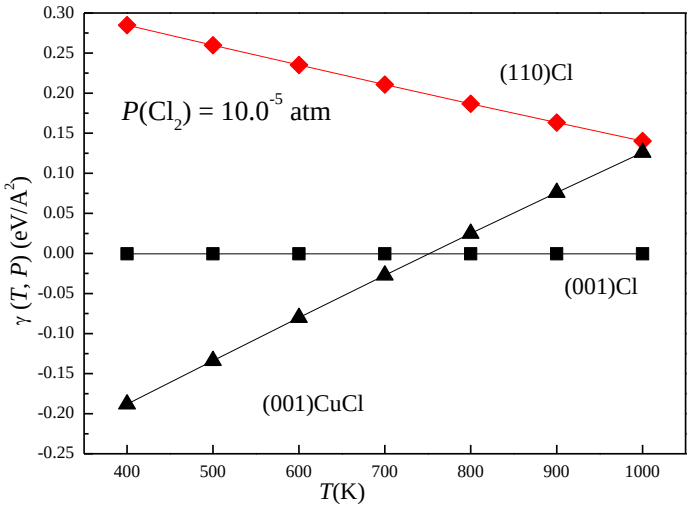

406

407 **Figure 5**. Surface free energies of the three most stable $CuCl_2$ configurations at P_{Cl2} = 1.0

408 ppm (a) and P_{Cl2} = 100.0 ppm (b).